Impact of vortex generator on gas turbine blade cooling application

Nirmal Halder,
Assistant profess, Aerospace Engineering,
Sandip University,
Nashik, Maharashtra, India
subho.nirmal@gmail.com

Abstract-Present numerical investigation proposes to mitigate the effects of Counter rotating vortex pair by employing vortex generator. The common-flow-down arrangement of delta winglet pair is preferred for this investigation Numerical simulation has been carried out to investigate the effect of placement of vortex generator on the characteristics of film cooling effectiveness. Repercussions, of utilizing multiple vortex generator at different downstream location have been detected. Result indicates that Vortex generator, located at up-stream of circular film cooling hole will yield better effectiveness. Reynolds number based on free stream velocity and film cooling-hole dimension is kept at 17000. Moreover consequence, in variation of blowing ratio, density ratio, secondary flow velocity or jet velocity and Turbulent Kinetic Energy on cooling effectiveness has been investigated. Result shows that increment in blowing ratio, jet velocity and Turbulent Kinetic Energy responsible for decrement in cooling effectiveness. The results are compared with baseline case. It has been observed that numerical investigation implementing FLUENT commercial code adopting the k-omega turbulence model perform better.

Keywords-Vortex generator, Film cooling, Common-flow-down, counter-rotating vortex pair, Delta winglet pair

I. INTRODUCTION

The intake temperature of a gas turbine determines its power output. Film cooling is utilized when input temperatures goes above the melting point of gas turbine components. Gas turbine components are protected from high intake temperatures by film cooling. The development of the counter rotating vortex pair (*CRVP*) is caused by the interaction of cold and hot fluids. *CRVP* directs hot air towards the turbine blade wall while also directing cool fluid away from the blade towards heated surroundings. As a result, *CRVP* reduces the efficiency of film cooling effectiveness. The primary fluid bends the secondary flow. *CRVP* is formed as a result of this phenomena. The longitudinal vortex (*LV*) is formed by the angle of attack. By installing an upstream ramp with ramp angles, Chen et al. [1] utilized an infrared imaging method to increase the film cooling performance. With an upstream ramp, Barigozzi et al. [2] used an infrared imaging method on cylindrical and fan-shaped film cooling holes. An increase in adiabatic efficiency was found when Na and Shih [3] provided a backward facing upstream ramp. Particle image velocimetry (*PIV*) and pressure sensitive paint (*PSP*) were used by Zhou and Hu [4] to improve cooling efficiency by utilizing a Barchan dune shaped ramp upstream and downstream of the film hole. Yao et al. [5] used numerical inspection whereas Dhungel et al. [6], Kapadia et al. [7] and Sargison et al. [8] used experimental research. Vortex generator enhances film cooling effectiveness [9]. Present study is performed implementing identical geometry of Halder et al. [10]. Vortex generator augments film cooling by creation of secondary vortices [11].

II.NOVELTY

Gas turbine blade film cooling is achieved implementing vortex generator in common flow down (CFD) configuration. Very few study is accomplished with VG is located at different upstream, downstream position. Less communication between primary and secondary flow presents inferior mixing resulting in low CRVP effect. Low CRVP effect signifies higher effectiveness. Very few studies demonstrate about the mitigation of CRVP implementing vortex generator. Current study deals with the mitigation of CRVP. CRVP is responsible for low effectiveness. Present investigation mitigates CRVP by creating secondary vortices originated from the vortex generator.

III. PROBLEM FORMULATION

Our assumption is fluids are Newtonian fluid and physical properties are invariant. For present study energy equations and Reynolds Averaged Navier-Stokes (RANS) are used. RANS can be divided into steady and unsteady RANS. Steady RANS (SRANS) is found to be unsuitable for predicting the flow field .However, for obtaining URANS solution initially we have to take the assistance of SRANS.

A. Computational domain and grid distribution

Dimensions are expressed with assist of film-hole diameter, D in figure 1-(a-f). Delta winglet pair (*DWP*) has been located at various upstream and downstream position (Table 1). The angle of attack, φ is 15 degrees. Grid arrangement has been shown in Figure 1-(h). Finer grids are used in the DWP region and film cooling hole region. However figure 1-(g) and (h) represents boundary condition and geometrical view respectively.

Table I. Details of configuration and position of DWP (VG) (See Figure 1(a-f)).

	1 DWP before hole (upstream)	1 DWP after hole (downstream)	1 DWP before and after the hole (up and downstream)	2 DWP after hole (downstream)	3 DWP after hole (downstream)
Figure 1-(a) (Baseline)	X	X	X	X	X
Figure 1-(b)	√	X	X	X	X
Figure 1-(c)	X	√	X	X	X
Figure 1-(d)	X	X	√	X	X
Figure 1-(e)	X	X	X	√	X
Figure 1-(f)	X	X	X	X	√

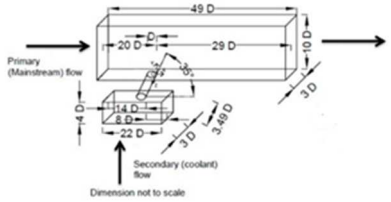

(a)

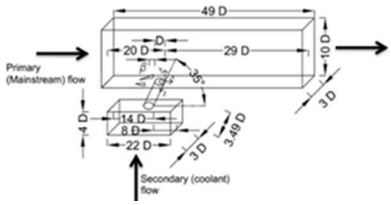

(b)

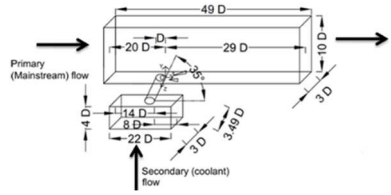

(c)

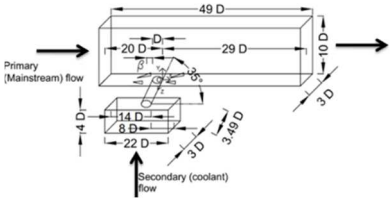

(d)

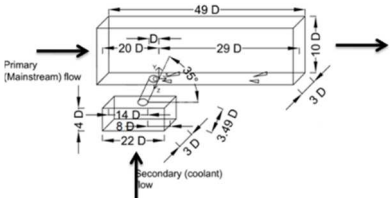

(e)

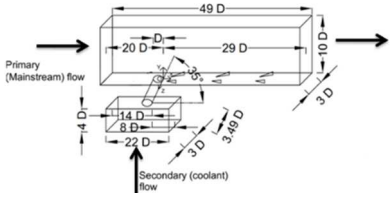

(f)

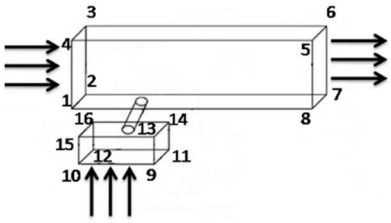

(g)

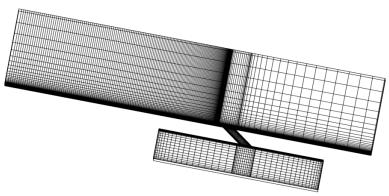

(h)

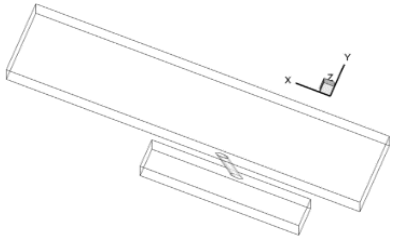

(i)

Fig. 1. (a), (b), (c), (d), (e), (f) graphic representation of computational domain and its bottom wall, (g) boundary condition, (h) grid distribution, (i) geometrical view

B. Choice of turbulence model

Several turbulence models have been investigated (k-ε standard, k-ε RNG, k-ε realizable, k-ω standard, and k-ω *SST*). The k-ω *SST* model outperforms all other turbulence models in terms of effectiveness distribution. Because of the development of primary vortices (*CRVP*) of the lowest strength, the k-ω *SST* model displays lower jet lift-off than the other turbulence models. Centerline as well as span line effectiveness are shown in figure 2. For the k-ω *SST* model, the most *CRVP* destruction occurred due to the opposing rotation of secondary vortices against *CRVP*.

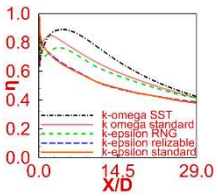

(a)

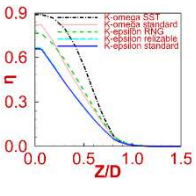

(b)

Fig. 2. Distribution of (a) Centreline and (b) span effectiveness for different turbulence model: K-epsilon standard, K-epsilon realizable, K-epsilon RNG, K-omega standard, K-omega SST.

C. Governing equation

A three-dimensional simulation is performed to solve governing equation. Primary assumption is fluids are Newtonian fluid and physical properties are invariant. For present study Reynolds Averaged Navier-Stokes (RANS) and energy equations are used. RANS can be divided into steady and unsteady RANS. Steady RANS (SRANS) is found to be unsuitable for predicting the flow field. Unsteady RANS (URANS) predicts well the flow involving adverse pressure gradient, airfoil and transonic shock waves. In dimensionless form continuity, momentum and energy equations defined as

$$\frac{\partial \overline{u_i}}{\partial x_i} = 0 \tag{1}$$

$$\frac{\partial \overline{u_i}}{\partial t} + \frac{\partial (\overline{u_i u_j})}{\partial x_j} = -\frac{\partial \overline{p}}{\partial x_i} + \frac{1}{\mathrm{Re}} \frac{\partial^2 \overline{u_i}}{\partial x_j^{\,2}} + \frac{\partial \tau_{ij}}{\partial x_j} \tag{2}$$

$$\frac{\partial \overline{\theta}}{\partial t} + \frac{\partial \left(\overline{u_j \theta}\right)}{\partial x_j} = \frac{1}{\mathrm{Re}\,\mathrm{Pr}} \frac{\partial^2 \overline{\theta}}{\partial x_j^{\,2}} + \frac{\partial q_j}{\partial x_j} \tag{3}$$

Where $\tau_{ij} = -\overline{u_i' u_j'}$ and $q_j = -\overline{u_j' \theta'}$

Transport equations can be defined as

$$\frac{\partial}{\partial \mathrm{t}}(\rho k) + \frac{\partial}{\partial x_i}(\rho k u_i) = \frac{\partial}{\partial x_j}\left(\Gamma_k \frac{\partial k}{\partial x_j}\right) + G_k - Y_k \tag{4}$$

$$\frac{\partial}{\partial t}(\rho\omega)+\frac{\partial}{\partial x_i}(\rho\omega u_i)=\frac{\partial}{\partial x_j}\left(\Gamma_\omega\frac{\partial\omega}{\partial x_j}\right)+G_\omega-Y_\omega+D_\omega \quad (5)$$

Non-dimensional length, velocity, time and temperature scale is film hole diameter (D), jet velocity (u_j), D/u_j and $\theta=(T-T_{cf})/(T_j-T_{cf})$ respectively. Here T_j and T_{cf} specifies coolant jet and cross-flow temperature respectively. Here $\tau_{ij}=-\overline{u_i'u_j'}$ is turbulent stress (Reynolds stress tensor) and $q_j=-\overline{u_j'\theta'}$ is turbulent heat flux. ANSYS-FLUENT [12] provides extra information on *k- ω SST* model. Re, Pr represents Reynolds & Pradntl number. For the current investigation Pr is taken as 0.85.

D. Boundary Condition

Figure 1-(g) and Table 2 present Boundary condition. Primary velocity (u_α *or* u_{cf}) of 104 *m/s* and 2.54 mm film cooling hole diameter (D) is utilized for a constant Reynolds number ($u_\alpha D/\nu$) of 17000. Here blowing ratio ($M=\rho_j u_j/\rho_{cf}u_{cf}$) is kept as 1. Cross-flow inlet temperature kept as 300 *K* and film-hole outlet temperature has been considered as 150 *K*. Outflow conditions have been used for the outlet. Symmetry and no-slip adiabatic wall boundary condition is provided for top and bottom wall surface respectively. For cross and jet flow domain the application of periodic boundary condition is done in span wise direction. Adiabatic wall boundary condition has been implemented for other faces and coolant hole. TI is turbulent intensity. 1.75% TI for cross flow, 5.5% TI for jet flow.

Table II. Boundary conditions (shown in Figure 1(g))

Boundaries	Boundary conditions
1-2-3-4, 9-10-12-11	Velocity: Velocity inlet (104 m/s of crossflow, 52 m/s of jet for M=0.5), Temperature: 300 K for cross flow, 150 K for jet flow.
5-6-7-8	Outflow
1-4-5-8, 2-3-6-7, 10-15-13-9, 12-16-14-11	Periodic
5-6-3-4	Symmetry
8-7-2-1	Velocity: wall (No slip), Temperature: wall (adiabatic)
9-13-14-11, 10-12-16-15	Velocity: wall (No slip), Temperature: wall (adiabatic)
Vortex generator, pipe	Velocity: wall (No slip), Temperature: wall (adiabatic)

E. Grid independence and convergence analysis

Grid independence was carried out as mentioned in Figure 3. Fine mesh is kept near the wall so that it can solve the laminar sub layer. Three type of meshes are considered for this investigation namely coarse (3424674 numbers of cells), intermediate (4231732) and fine (5323721). Grid independence and convergence study has been performed with earlier mentioned meshes. Little disparity is noticed between coarse, intermediate and fine grid results. For subsequent simulation fine grid has been considered.

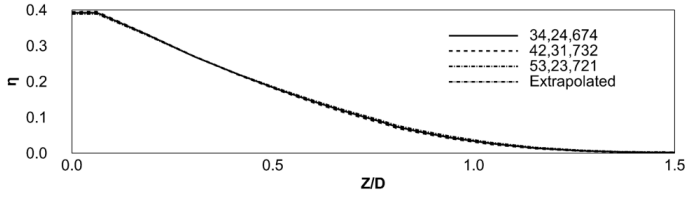

Fig. 3. Grid independence study

F. Simulation procedure

FLUENT, a commercial computational fluid dynamics code, is used to solve the governing equations. With the help of ICEMCFD, an unstructured mesh was created. The SIMPLE algorithm is used to link pressure and velocity. The second-order upwind technique is used to discretize momentum, energy, turbulent dissipation rate, and turbulent kinetic energy. Convergence criteria is preserved at order of 10^{-6} for continuity and momentum equations, whereas it is set at 10^{-8} for energy equation. Apart from that, the turbulent kinetic energy dissipation convergence criteria is kept at order of 10^{-6}. The convergence was validated by observing the temperature and velocity variations as a function of iteration number and mass balance.

G. Validation study

For the validation research, the baseline was compared to the experimental inquiry. Figure 4 depicts the effectiveness distribution along the centerline. For the purposes of this investigation, the averaged value in the span-wise direction was used.

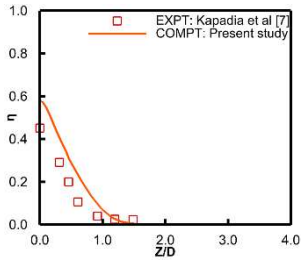

Fig. 4. Effectiveness at X = 15D in the baseline Validation study

IV. RESULT AND DISCUSSION

The mechanism for mitigation of CRVP has been discussed. Here maximum CFL (courant friedrichs levy) is calculated as ($u\Delta t/\Delta x$). Where u, describes maximum velocity (m/s), Δt presents time step size (s) and Δx defines as minimum grid size (m). Maximum CFL is estimated as 1, where Δt is kept as 10^{-5} second.

A. Effect of distance between film cooling hole and vortex generator

1) Temperature distribution at cross-sectional plane

Non-dimensional temperature distribution for mid-plane (Z/D = 0) is depicted in Figure 5. Lower jet lift-off is noticed in X/D=7.89 (Figure 5-(b)), as a result higher cooling effectiveness is observed for lower distance among film hole & VG. Which (lower distance among film hole & VG) is responsible for lower jet lift-off. This lower jet lift-off may be attributed to downwash flow, lower CRVP effect.

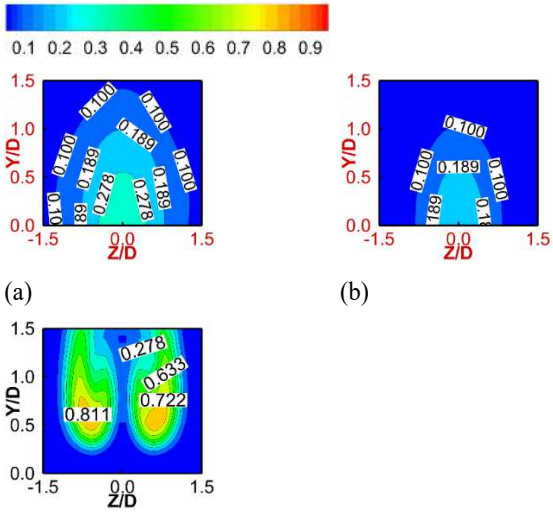

Fig. 5. Non-dimensional temperature distribution for cross plane (X/D = 10) for distance between trailing edge of film cooling and vortex generator. VG located at X/D = (a) 9.81, (b) 7.89 and (c) baseline

B. Effect of increase in the vortex generator

Effects of an increase in vortex generator (VG) have been discussed with cross-plane vector distribution. The RMS (root mean square) value reduces with an increase in number of VG indicating a reduction in amplitude of fluctuation for increment in VG as compared to baseline.

1) Vector distribution

From the vector distribution in Figure 6, with increment in the vortex generator results increase in bottom wall effectiveness which may be attributed to a decrease in the strength of CRVP. The lower strength of CRVP results in decreases in jet lift-off.

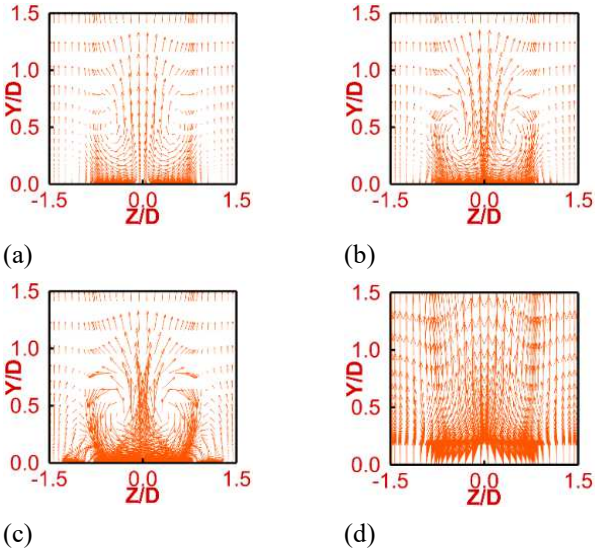

Fig. 6. Vector distribution for increment in DWP. (a) DWP=1, (b) DWP=2, (c) DWP=3 and (d) baseline at X/D = 10

C. Effect of vortex generator's length

Careful examination may express that an increment in bottom wall effectiveness has been inspected with increments in vortex generator length. However, from cross-plane temperature distribution almost similar kind of information has been received.

1) Bottom wall effectiveness distribution

Higher vortex generator length responsible for the formation of lower strength of CRVP resulting higher bottom wall effectiveness (Figure 7). This may be attributed to the lower ventilation of heated cross flow beneath the cold jet from span wise direction.

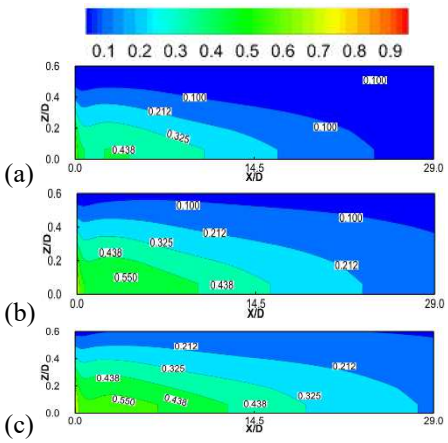

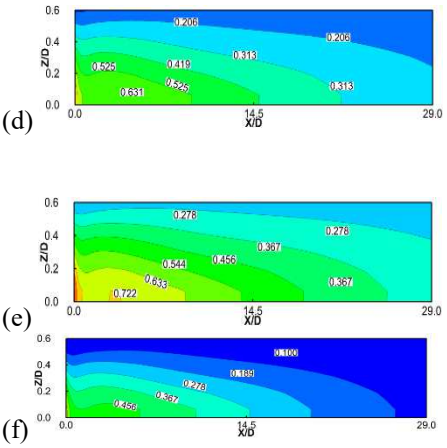

Fig. 7. Bottom wall effectiveness distribution for different VG length. (a) 3.07D, (b) 4D, (c) 4.47D, (d) 4.94D and (e) 6.76D and (f) baseline.

D. Effect of vortex generator's height

With the enhancement of VG height greater bottom wall effectiveness is inspected. Usually we take the height of vortex generator in terms of boundary layer thickness. Here height is taken in terms of film cooling hole diameter. But we cannot go beyond a certain limit due to having pressure drop associated with height.

1) CRVP distribution

Strength of primary vortices (CRVP) reflects up-ward movement of vortex core as shown in Figure 8. Lower strength of CRVP retains the cold fluid near to the bottom wall as a consequence we are obtaining higher effectiveness. Higher strength of CRVP accountable for higher jet lift-off.

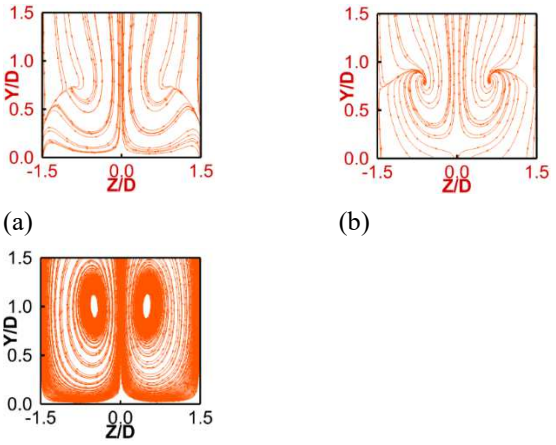

Fig. 8. CRVP distribution for different VG height. (a) 2 D, (b) 2.25 D and (c) baseline at X/D = 10

E. Effect of Reynolds number

Effect of Reynolds number have been discussed with centerline & span line effectiveness distribution at cross-sectional plane.

1) Centerline & span-line effectiveness

Figure 9 describes centerline and span line effectiveness. Higher effectiveness takes place at lower Reynolds number as mentioned in Figure 9. Blowing ratio increases with increase of Reynolds number. The Lower Reynolds number depicts the lower velocity of jet. The lower velocity of jet remains longer period close to the bottom wall. As a result coolant spread over the bottom wall in span and downstream direction. Higher cooling region is detected at the bottom wall results higher effectiveness at low Reynolds number (Re = 15000)

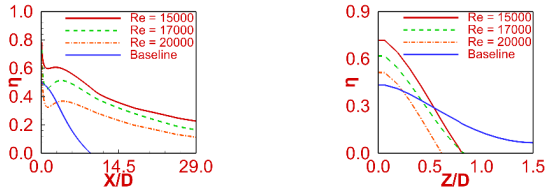

(a) (b)

Fig. 9. (a) centerline effectiveness, (b) span line effectiveness at X/D = 10 for Re = 15000, 17000, 20000

F. Effect of turbulent intensity

The effect of turbulent intensity (TI) have been explained with CRVP distribution (Figure 10).

1) Temperature distribution at mid plane

Figure 10 explain that a decrease in TI, will be responsible for a decrease in jet lift-off. A decrease in jet lift-off allows cold fluid to stay near the bottom wall resulting higher cooling effect. Lower turbulent intensity indicates lower mixing between primary and secondary flow resulting lower CRVP effect. The low detrimental effect of CRVP is responsible for higher cooling effect.

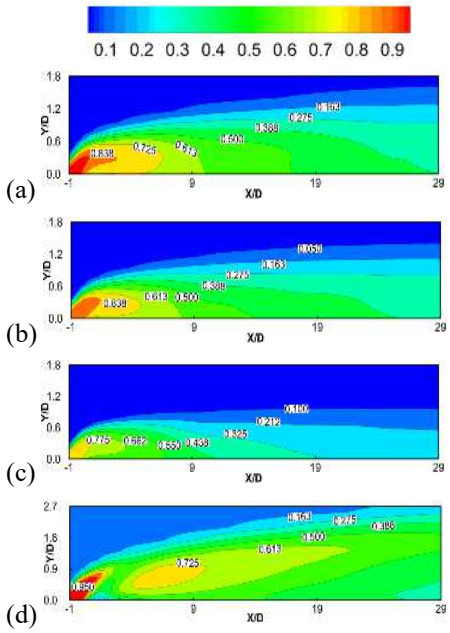

(a) (b) (c) (d)

Fig. 10. Non-dimensional temperature distribution at mid plane

For TI = (a) 15, (b) 10, (c) 5 and (d) baseline

G Effect of location

Effect of location is discussed with bottom wall effectiveness distribution.

1) Bottom wall effectiveness distribution

From bottom wall effectiveness distribution in Figure 11, it is quite evident that best film cooling effectiveness has been achieved with DWP located at before the hole while the lower effectiveness accomplished with DWP positioned at after the film hole. Lowest effectiveness achieved with baseline case.

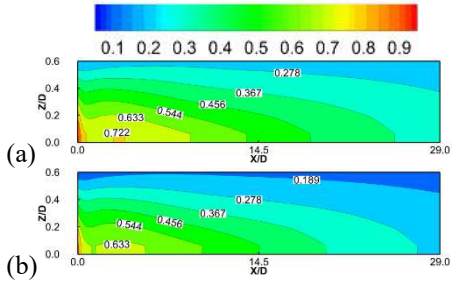

(a) (b)

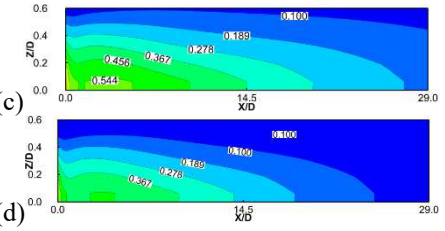

(c) (d)

Fig. 11. Effectiveness distribution of bottom wall for *DWP* located at (d) before (e) before and after, (f) after film hole and (g) baseline

H Effect of blowing ratio

Effect of blowing ratio (M) is discussed with centerline and span line effectiveness.

1) Centerline and span line effectiveness

Span line and centerline effectiveness for various M is depicted in Figure 12. It represents higher centerline and span effectiveness distribution for lower blowing ratio. This may be attributed to creation of downwash flow due to CFD configuration. Downwash flow represents lower jet lift-off, less lateral ventilation of hated cross flow, low CRVP effect, inferior mixing between primary and secondary flow resulting greater effectiveness.

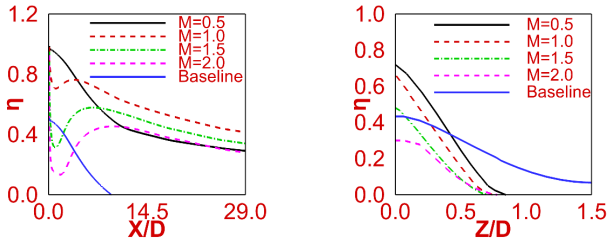

(a) (b)

Fig. 12. (a) Centreline effectiveness, (b) span line effectiveness at X/D = 10 for different in *M*

I Effect of density ratio

Effect of density ratio (DR) is discussed with vector distribution.

1) Vector distribution

From vector distribution (Figure 13) it is easily observed that boost in D.R, enhances the cooling effect by destroying CRVP. For this reason greater bottom wall effectiveness is obtained for highest D.R. Also when density ratio enhances then decrease in blowing ratio is observed. Lower blowing ratio indicates lower velocity of cold jet flow. As a result higher cooling effectiveness is perceived.

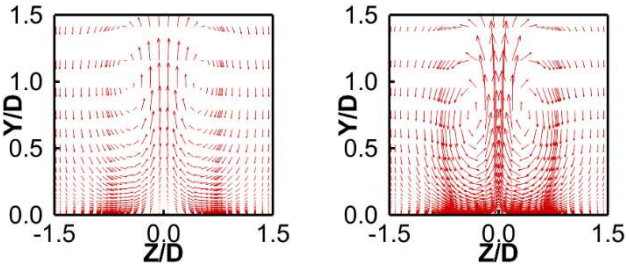

(a) (b)

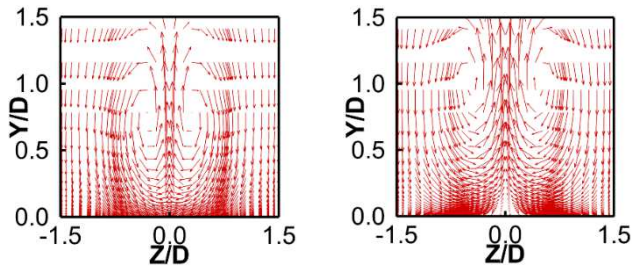

Fig. 13. Vector distribution for different density ratio, DR= (a) 0.5, (b) 1.0, (c) 2.0 and (d) baseline at X/D = 10

J Effect of jet inlet velocity

Effect of jet inlet velocity (u_j) is discussed with mid plane non-dimensional temperature, cross plane non-dimensional temperature and vector distribution. Effect of u_j is also discussed with bottom wall effectiveness distribution.

1) CRVP distribution

From CRVP distribution (Figure 14) it is easily observed that with the boost in u_j, strength of primary vortices (CRVP) will be enhanced. This ultimately decreases the cooling effect by minimizing cooling region. For this reason greater bottom wall effectiveness is obtained for lowest u_j. When u_j decreases then decrease in blowing ratio is observed. Lower blowing ratio indicates lower velocity of cold jet flow.

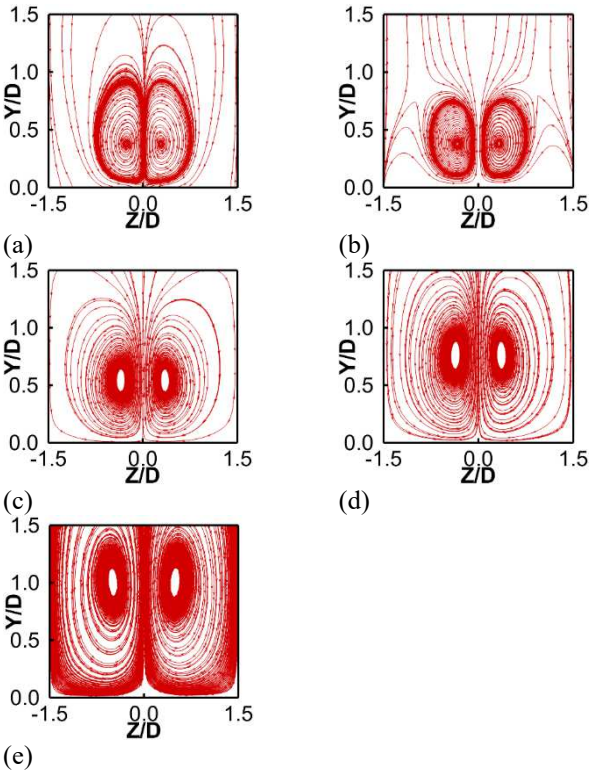

Fig. 14. CRVP distribution for different jet inlet velocity, u_j = (a) 0.236, (b) 0.471, (c) 0.707, (d) 0.942 and (e) baseline at X/D = 10

K. Effect of Turbulent Kinetic Energy

Effect of Turbulent kinetic energy (T.K.E) is discussed with mid plane non-dimensional temperature.

1) Non dimensional Temperature distribution at mid plane

Figure 15 exemplifies enhancement in jet lift off with boost in T.K.E. Increase in T.K.E indicates decrement in cooling effect at mid plane. Enhancement in jet lift-off assists to send the cold fluid to the hot environment which decreases the bottom wall effectiveness. Which may be attributed to the greater interaction between primary and secondary flow with the enhancement in T.K.E. Low T.K.E responsible for the less ventilation of cross flow and less detrimental effect of CRVP. Detrimental effect of CRVP is, it brings the hot mainstream air towards bottom wall, increasing the turbine blade wall temperature resulting lower film cooling effectiveness. CRVP is responsible for jet lift-off.

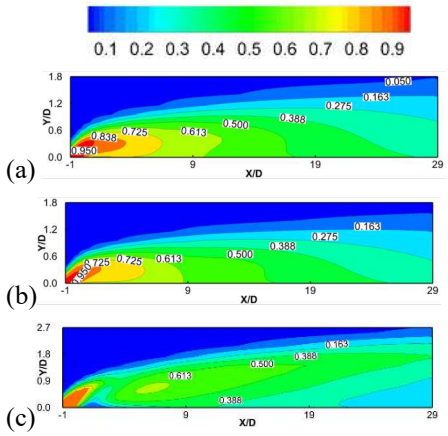

Fig. 15. Non-dimensional temperature distribution at mid plane for different Turbulent Kinetic Energy, *TKE* = (a) Low, (b) High, and (c) baseline at *X/D* = 10

V. CONCLUSIONS

A simulation study has been carried out to investigate the effect of common flow down delta winglet pair configuration on film cooling effectiveness of gas turbine blade. Unsteady Reynolds averaged Navier-Stokes equation. Among the various turbulence models, K-ω SST model exhibits best effectiveness distribution. Reynolds number has been fixed at 17000. Time-averaged velocity field, temperature field and vector distribution results are reported in this study.

Major findings are:

1. Higher film cooling effectiveness is observed for delta winglet pair configuration compared to the baseline case.
2. Highest film cooling effectiveness is observed at blowing ratio of 0.5.
3. Position of VG both in upstream and downstream are also investigated to explain the effect of DWP. Best effectiveness has been achieved with DWP located at before the hole while for the worst is observed with DWP located at after the hole.

NOMENCLATURE

CRVP	Counter rotating vortex pair
M	Blowing ratio
ρ_j	Density of jet [kg.m^{-3}]
u_j	Jet exit velocity [m.s^{-1}]
ρ_{cf}	Density of cross flow [kg.m^{-3}]
u_{cf}	Cross flow inlet velocity [m.s^{-1}]
η	Film cooling effectiveness $(\boldsymbol{T}-\boldsymbol{T_{cf}})/(\boldsymbol{T_j}-\boldsymbol{T_{cf}})$
T_{aw}	Adiabatic wall non-dimensional temperature [K]
T_{cf}	Cross flow inlet non-dimensional temperature [K]
T_j	Non-dimensional temperature of jet [K]
VG	Vortex generator
TV	Transverse vortices

LV	Longitudinal vortices
β	Distance of DWP from leading edge of hole in down as well as upstream direction.
φ	The angle of attack [^{O}]
DR	Density ratio
TKE	Turbulent kinetic energy [$m^2.s^{-2}$]
LVGs	Longitudinal vortex generators
WP	Winglet pair
DWP	Delta Winglet pair
TI	Turbulent intensity
DWs	Delta wings
D	Diameter of jet [mm]
ν	Dynamic viscosity [$N.s.m^{-2}$]
Re	Reynolds number
X/D	Ratio of downstream distance from the centre of the film hole to film diameter
Z/D	Ratio of transverse distance from the centre of the film hole to film diameter
U	Stream wise velocity [$m.s^{-1}$]
V	vertical velocity [$m.s^{-1}$]
W	Span wise velocity [$m.s^{-1}$]
CFU	Common-flow-up
CFD	Common-flow-down
Non-dimensional temperature	$(\boldsymbol{T - T_{cf}})/(\boldsymbol{T_j - T_{cf}})$

REFERENCES

[1] P. Chen, K. Chya, P. Shih, (2011). Effects of upstream ramp on the performance of film cooling. International journal of thermal sciences 50: 1085-1094.

[2] G. Barigozzi, G. Franchini, and A. Perdichizzi, (2007). The Effect of an Upstream Ramp on Cylindrical and Fan Shaped Film Cooling Hole Film Cooling—Part II Adiabatic Film Cooling Effectiveness. ASME Paper No: GT2007-27079.

[3] S. Na, and T. Shih, (2007). Increasing Adiabatic Film Cooling Effectiveness Using an Upstream Ramp. ASME J. Heat Transfer. 129: 464–471.

[4] W. Zhou, and H. Hu, (2016). Improvements of film cooling effectiveness by using Barchan dune shaped ramps. International Journal of Heat and Mass Transfer 103: 443-456.

[5] Jun Yao, Yufeng Yao, (2011). Computational study of hole shape effect on film cooling performance. Proc. IMechE Part A: Journal of Power and Energy 225: 1-14.

[6] A. Dhungel, Y. Lu, W. Phillips, S. V. Ekkad, J. Heidmann (2002). Film cooling from a row of holes supplemented with anti-vortex holes. Journal of Turbomachinary. 131(2): 021007 1-10.

[7] S. Kapadia, S. Roy and J. Heidmann, (2003). Detached eddy simulation of turbine blade cooling. In 36th AIAA Thermophysics Conference, AIAA-2003-3632, Orlando, Florida: 23–26.

[8] J.E. Sargison, (2001). Development of a novel film cooling hole geometry. PhD Thesis, 2001 (University of Oxford).

[9] N. Halder, A. Saha, P. K. Panigrahi, (2020). Enhancement in Film Cooling Effectiveness Using Delta Winglet Pair. Journal of thermal science and engineering application 13: 1-17.

[10] N. Halder and P. K. Panigrahi, (2021). Cooling performance of vortex generator. Proceedings of the Institution of Mechanical Engineers, Part A: Journal of Power and Energy 235: 1619-1638.

[11] N. Halder, A. K. Saha, and P. K. Panigrahi. (2017), Influence of Delta Wing Vortex Generator on Counter Rotating Vortex Pair in Film Cooling Application of Gas Turbine Blade. Fluid Mechanics and Fluid Power–Contemporary Research. Springer, New Delhi: 95-103.

[12] ANSYS FLUENT User's Guide.